Advances in Aerodynamics

RESEARCH Open Access

Effect of thermal fluctuations on homogeneous compressible turbulence

Qihan Ma[1], Chunxin Yang[1], Song Chen[2], Kaikai Feng[1] and Jun Zhang[1*]

*Correspondence: jun.zhang@buaa.edu.cn

[1] School of Aeronautic Science and Engineering, Beihang University, Beijing 100191, China
[2] Sino-French Engineer School/School of General Engineering, Beihang University, Beijing 100191, China

Abstract

For more than a century, it has been widely believed that there is a clear gap between molecular motions at the microscopic level and turbulent fluctuations at the macroscopic level. However, recent studies have demonstrated that the thermal fluctuations resulted from molecular motions have nonnegligible effects on the dissipation range of turbulence. To further clarify the reviving debate on this topic, we employ the molecular-level direct simulation Monte Carlo (DSMC) method to simulate homogeneous turbulence with different turbulent Mach numbers, extending the previous studies by considering the effect of compressibility. Our results show that, for both one-dimensional (1D) stationary turbulence and two-dimensional (2D) decaying isotropic turbulence, the turbulent energy spectra are significantly changed due to thermal fluctuations below the spatial scale comparable to the turbulent dissipation length scale. The energy spectra caused by thermal fluctuations for different spatial dimensions d present different scaling laws of the wavenumber k as $k^{(d-1)}$. For 2D cases, we show that the effect of thermal fluctuations on the spectrum of compressible velocity component is greatly affected by the change of compressibility. The 2D spectra of density, temperature and pressure are also obtained, showing the same scaling law at large wavenumbers as found for the energy spectra. Moreover, it is found that the effects of thermal fluctuations on the thermodynamic spectra are the same as those on the spectra of compressible velocity component.

Keywords: Thermal fluctuations, Homogeneous compressible turbulence, DSMC, Turbulent Mach number, Energy spectrum

1 Introduction

Turbulence is characterized by the random fluctuations of flow fields in both space and time [1]. It is known that the spectrum of turbulent velocity fluctuations inherently reflects the so-called "energy cascade", which describes the successive transfer of turbulent kinetic energy (TKE) from the largest scales to the smaller ones. The characteristic length scale below which TKE is dominantly dissipated by the viscosity is defined as the Kolmogorov length scale [1, 2]

$$\eta = \left(\frac{\nu^3}{\varepsilon}\right)^{1/4}, \tag{1}$$

where ν is the mean kinematic viscosity, and ε is the mean dissipation rate per unit mass.

As the scale of turbulence continuously decreases, it is natural to ask whether the molecular effects contribute to the turbulent motions. This question for gases can be roughly answered by estimating the ratio of the molecular mean free path, λ_{mic}, to the Kolmogorov length scale as [2, 3]

$$\frac{\lambda_{mic}}{\eta} = \hat{C}\frac{M_t}{{Re_T}^{1/4}}, \tag{2}$$

where M_t is the turbulent Mach number, Re_T is the turbulent Reynolds number, and $\hat{C}$ is a constant in the same order of magnitude as 1. Equation (2) indicates that $\eta \gg \lambda_{mic}$ for low-Mach-number, and high-Reynolds-number turbulence. Under this condition, it is widely believed that the microscopic molecular motions have negligible effects on the macroscopic turbulent fluctuations, and the Navier-Stokes (NS) equations can accurately describe the turbulent fluctuations at all scales.

However, there have been a few researches presenting a different point of view. In the seminal work of Betchov [4, 5], he anticipated that the spontaneous thermal fluctuations resulted from molecular motions would act on length scales larger than the molecular mean free path and may have significant effects on the dissipation range of turbulence. Note that this conjecture cannot be validated based on the deterministic NS equations.

To investigate the effect of thermal fluctuations on turbulent flows, one can turn to the fluctuating hydrodynamic equations, which were first proposed by Landau and Lifshitz [6]. By adding stochastic fluxes into the deterministic hydrodynamic equations, the fluctuating hydrodynamic equations are capable of describing the thermal fluctuations at the mesoscopic level [7, 8]. Recently, Bell et al. [9] simulated the three-dimensional (3D) incompressible homogeneous isotropic turbulence by solving fluctuating Navier-Stokes (FNS) equations. They found that in the turbulence dissipation range, the exponentially decaying turbulent kinetic energy spectrum predicted by the deterministic NS equations [10, 11] is altered by the thermal fluctuations, which result in the spectrum growing quadratically with the wavenumber k. The crossover wavenumber k_c at which the thermal fluctuations start to dominate the spectrum is in the same order of magnitude as the Kolmogorov wavenumber k_η. Besides, the strong intermittency in the turbulence far-dissipation range predicted by the deterministic NS equations [12, 13] is also replaced by the Gaussian thermal equipartition [9, 14].

Since thermal fluctuations are inherently caused by molecular random motions, the molecular-level simulation approaches, such as the molecular dynamics (MD) method [15, 16] and the direct simulation Monte Carlo (DSMC) method [17], can provide a more straightforward and physically reasonable way to study the effect of thermal fluctuations. MD is a deterministic method which simulates the movement of physical real molecules/atoms following Newton's equations of motion [15]. The interactions between molecules/atoms are accurately calculated based on the interatomic potentials. In contrast, the DSMC method is a stochastic approach, in which each simulated molecule statistically represents a fixed number of real molecules [17, 18]. Besides, the intermolecular collisions in the DSMC method are treated stochastically using phenomenological models [19]. These characteristics make the DSMC method much more efficient than MD in simulating gas flows. Theoretically, the DSMC method is proved to be a particle

algorithm for solving Boltzmann equation of monatomic gases [20], and this method has been successfully applied to investigate the thermal fluctuation phenomena [21–26].

With the rapid development in high performance computing, it has become possible to use the DSMC method to study continuum flow problems, such as the hydrodynamic instability [27–30] and turbulence [31–35]. For turbulence simulations, previous studies have demonstrated that the turbulent statistics obtained by the DSMC method, such as TKE and ε, are in good agreement with those obtained by the direct numerical simulation (DNS) method based on the deterministic NS equations [31, 33]. To further study the effect of thermal fluctuations on turbulence, McMullen et al. [35] simulated the 3D decaying Taylor-Green (T-G) vortex flow, and they obtained the same k^2 dependence energy spectrum at the large wavenumbers as that predicted by the FNS calculations [9], indicating the significant effect of thermal fluctuations on the turbulent dissipation range. It is also found that, at the late stage of T-G flow decay, the velocity field simulated by DSMC shows great irregularity comparing to that obtained from the deterministic DNS method [33], and this irregularity is caused by the thermal fluctuations.

It is worth noting that the previous works on the effect of thermal fluctuations on turbulence [9, 14, 35] mainly focus on the incompressible turbulence, and the discussions are limited to the turbulent velocity fluctuations. For compressible turbulence, the divergence of the velocity field is non-zero, leading to the compression and expansion effects of the velocity field in addition to the shear and eddy motions [36, 37]. Besides, a unique feature of the compressible turbulence is the fluctuations of thermodynamic variables, such as density, temperature, and pressure [38]. The coupling between fluctuating thermodynamic variables and the turbulent velocity field has been widely studied based on the compressible deterministic NS equations [38–43]. Considering the molecular effect on turbulence, it is noteworthy that the Kolmogorov length scale may get close to the molecular mean free path at large turbulent Mach numbers (see Eq. (2)). This implies that the local thermodynamic equilibrium (LTE) assumption inherent in the FNS equations may break down, especially when shocks occur in the high-Mach-number turbulence [14]. Since the DSMC method makes no assumption of LTE [35], it can be employed to simulate highly compressible turbulence with strong nonequilibrium effects.

In this work, the DSMC method is employed to simulate the homogeneous compressible turbulence. The aim of this work is to study the effect of thermal fluctuations on turbulence with different M_t, by examining the spectra of both the velocity and thermodynamic variables. Specifically, the one-dimensional (1D) stationary turbulence is simulated, and the effect of thermal fluctuations on the turbulent energy spectra is investigated. Then, the two-dimensional (2D) decaying isotropic turbulence is simulated. By applying the Helmholtz decomposition to the velocity field [40], the effect of thermal fluctuations on the solenoidal and compressible velocity components can be investigated separately. The spectra of the fluctuating thermodynamic variables are further studied.

The remainder of this paper is organized as follows. In Section 2, we briefly introduce the DSMC method, and then we describe some basic theories of thermal fluctuations under the DSMC framework. In Sections 3 and 4, we present our numerical investigations for the 1D stationary turbulence and the 2D decaying turbulence, respectively. Conclusions are drawn in Section 5.

2 Methodology

2.1 DSMC method

In this work, we employ the direct simulation Monte Carlo (DSMC) method [17] to simulate homogeneous turbulence of gases. Figure 1 shows the schematic of DSMC simulations, where the simulated molecules (displayed by orange spheres) move and collide with each other in a 3D periodic domain. As mentioned before, each simulated molecule statistically represents a fixed number F of identical real molecules, and F is the so-called simulation ratio [31, 35].

Although the simulated molecules move in a 3D computational domain, we can simulate 1D and 2D turbulent flows by dividing the domain into different types of computational cells. As shown in Fig. 1, the computational domain is divided into cells only in the y direction for 1D flow simulations, while both x and y directions are divided into cells for 2D flow simulations. The macroscopic gas properties are obtained locally for each cell by taking the instantaneous average of the corresponding molecular information [17, 18]. Specifically, the local number density n and macroscopic velocity $\vec{u}$ are given by

$$n = \frac{N_p F}{V_{cell}}, \tag{3}$$

$$\vec{u} = \frac{\sum_{i=1}^{N_p} \vec{c}_i}{N_p}, \tag{4}$$

where N_p is the number of simulated molecules in the computational cell, V_{cell} is the volume of the computational cell, and $\vec{c}_i$ is the molecular velocity. Note that the simulation ratio F appears in the numerator of Eq. (3), so n represents the number density of the real gas. For single-species gas, the mass density ρ can be calculated as $\rho = nm$, where m is the molecular mass. We further define the molecular thermal velocity as $\vec{C}_i = \vec{c}_i - \vec{u}$, and the local temperature T can be calculated as [17]

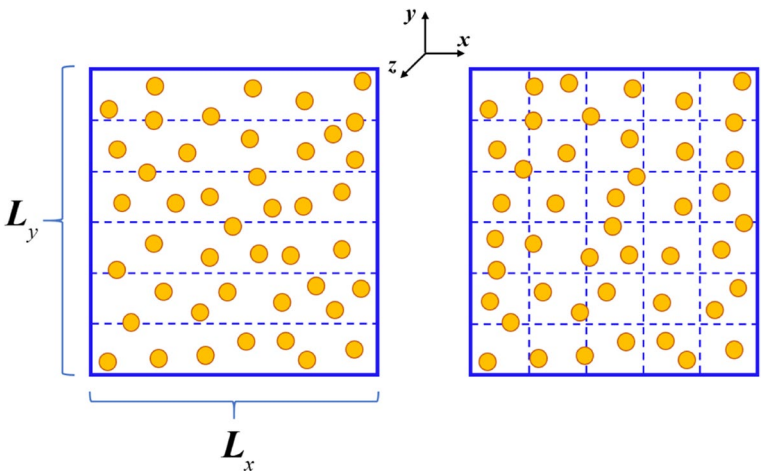

Fig. 1 Schematic diagram of DSMC simulations for 1D (left) and 2D (right) turbulence. The simulation domain is displayed in the $x - y$ plane

$$T = \frac{\sum_{i=1}^{N_p} \frac{1}{2} m \vec{C}_i^{\,2}}{\frac{3}{2} N_p k_B}, \tag{5}$$

where k_B is the Boltzmann constant. Assuming that the gas satisfies the ideal gas law, the local pressure P can be further calculated as $P = nk_BT$.

For the applications of the DSMC method, the first step is to generate simulated molecules according to the initial macroscopic conditions of the flow field. The following steps implement two sequential processes in each calculated time interval, i.e., the molecular motions and intermolecular collisions, which are assumed to be uncoupled. While the molecular motions are performed deterministically according to the molecular instantaneous velocities, the intermolecular collisions are implemented in a stochastic way based on the phenomenological models. Specifically, the widely used no-time-counter (NTC) technique [17] is employed to randomly choose molecules in the same cell as collision pairs, and the variable soft sphere (VSS) model [19] is used to determine the post-collision velocities of molecules.

In this work, we simulate turbulent flows of the argon gas, whose molecular mass $m = 6.63 \times 10^{-26}$ kg. The VSS model parameters of argon are shown in Table 1, where d_{ref} is the reference collision diameter at the reference temperature T_{ref}, α represents the scattering angle distribution of the collision, and ω is the so-called viscosity index. The local dynamic viscosity μ is calculated as [18]

$$\mu = \mu_{ref} \left(\frac{T}{T_{ref}} \right)^{\omega}, \tag{6}$$

where $\mu_{ref} = 2.117 \times 10^{-5}$ Pa · s is the reference viscosity of argon at T_{ref}=273.15 K [17]. The local thermal conductivity κ is determined from the viscosity μ as [18]

$$\kappa = \gamma \frac{\mu c_v}{Pr}, \tag{7}$$

where $\gamma = 5/3$ is the specific heat ratio, $c_v = 3R/2$ is the isochoric specific heat, R is the specific gas constant, and $Pr = 2/3$ is the Prandtl number. Using the VSS model parameters, we can further estimate the mean collision rate per molecule as [17]

$$\nu_{mic} = 4 {d_{ref}}^2 n \left(\frac{\pi k_B T_{ref}}{m} \right)^{\frac{1}{2}} \left(\frac{T}{T_{ref}} \right)^{1-\omega}, \tag{8}$$

and the molecular mean collision time is calculated as $\tau = 1/\nu_{mic}$. The molecular mean free path is defined as $\lambda_{mic} = C_{th}\tau$, where $C_{th} = \sqrt{8k_BT/\pi m}$ denotes the average thermal speed of molecules.

Table 1 VSS parameters of argon [17]

T_{ref} (K)	d_{ref}(Å)	α	ω
273.15	4.11	1.40	0.81

All the DSMC simulations are performed in the open-source code SPARTA [30, 44], which has been widely used in the simulation of rarefied gas flows as well as turbulent flows [31–35]. It should be emphasized that, to ensure the simulation accuracy, the simulation time step needs to be smaller than τ , and the cell length needs to be smaller than λ_{mic} [45, 46].

2.2 Spatial correlation of thermal fluctuations

In this subsection, the basic theory of thermal fluctuations under the framework of DSMC simulations is introduced. In general, the fluctuation of a macroscopic property a is defined as the deviation of its local instantaneous value from its mean, i.e., $\delta a(\vec{r},t) = a(\vec{r},t) - \langle a \rangle$. For gases at global thermodynamic equilibrium, fluctuations arise spontaneously due to the random thermal motions of molecules [24, 26].

According to the equilibrium statistical mechanics [47–49], the mean square value of the y-component velocity fluctuations for a DSMC simulation cell is given as

$$\left\langle (\delta u_y)^2 \right\rangle = \frac{k_B \langle T \rangle}{V_{cell} \langle \rho \rangle}, \tag{9}$$

where $\langle T \rangle$ and $\langle \rho \rangle$ are the mean temperature and mass density, respectively. For gases at equilibrium, the velocity components are independent and identically distributed, so Eq. (9) also holds for δu_x and δu_z [47]. For thermal fluctuations of the number density, temperature and pressure, their mean square values are given as

$$\left\langle (\delta n)^2 \right\rangle = \frac{\kappa_T k_B \langle T \rangle \langle n \rangle^2}{V_{cell}}, \tag{10}$$

$$\left\langle (\delta T)^2 \right\rangle = \frac{k_B \langle T \rangle^2}{c_v V_{cell} \langle \rho \rangle}, \tag{11}$$

$$\left\langle (\delta P)^2 \right\rangle = \frac{\gamma k_B \langle T \rangle}{V_{cell} \kappa_T}, \tag{12}$$

respectively, where $\langle n \rangle$ is the mean number density, $\kappa_T = 1/\langle P \rangle$ is the isothermal compressibility of the ideal gas, and $\langle P \rangle$ is the mean pressure.

In this work, we focus on the spatial correlation of fluctuations at two DSMC cell points $\vec{r}_1$ and $\vec{r}_2$. Due to the spatial homogeneity of fluctuations, the two-point autocorrelation function $\langle \delta a(\vec{r}_1,t) \delta a(\vec{r}_2,t) \rangle$ only depends on the relative distance $\vec{r} = \vec{r}_2 - \vec{r}_1$ [1]. For gases at equilibrium, the thermal fluctuations are generally delta-correlated [48], that is,

$$\mathcal{R}_a(\vec{r}) = \langle \delta a(\vec{r}_1,t) \delta a(\vec{r}_2,t) \rangle = \left\langle (\delta a)^2 \right\rangle \delta_{\vec{r}}\,, \tag{13}$$

where $\delta_{\vec{r}}$ is defined as

$$\delta_{\vec{r}} = \begin{cases} 1, & \vec{r} = 0 \\ 0, & \vec{r} \neq 0 \end{cases}. \tag{14}$$

To calculate the spectra of thermal fluctuations, we employ the discrete Fourier transform (DFT) of 1D and 2D as [50]

$$\mathcal{F}\{a(\vec{r})\} = A(\vec{k}) = \begin{cases} \text{1D}: A(k_y q_y) = \sum\limits_{j_y=0}^{N_c-1} a(j_y \Delta y) e^{-i(\frac{2\pi}{N_c}) j_y k_y} \\ \text{2D}: A(k_x q_x, k_y q_y) = \sum\limits_{j_x=0}^{N_c-1} \sum\limits_{j_y=0}^{N_c-1} a(j_x \Delta x, j_y \Delta y) e^{-i(\frac{2\pi}{N_c})(j_x k_x + j_y k_y)} \end{cases}, \tag{15}$$

where $\mathcal{F}\{\cdot\}$ denotes the DFT, and $\vec{k} = k_i q_i$ ($k_i = 0, 1, \cdots N_c - 1$) represents the discrete wave vector. q_x, q_y are the unit wavenumbers in x and y directions, respectively, which can be calculated as $q_i = 2\pi / L_i$, where L_i denotes the length of the simulation domain for direction i (see Fig. 1). $\vec{r} = j_i \Delta i$ ($j_i = 0, 1, \cdots N_c - 1$) represents the discrete space point, where $\Delta i = L_i / N_c$ denotes the cell length of direction i, and N_c is the simulation cell number. For 2D DSMC simulations, the numbers of cells divided in the x and y directions are the same in our work.

The energy spectrum $E(k)$ can be expressed by the DFT of two-point velocity autocorrelation function [1]:

$$E(k) = E(\left|\vec{k}\right|) = \begin{cases} \text{1D}: \frac{1}{2}\mathcal{F}\{\mathcal{R}_{u_y}\} \\ \text{2D}: \frac{1}{2}\left(\mathcal{F}\{\mathcal{R}_{u_x}\} + \mathcal{F}\{\mathcal{R}_{u_y}\}\right) \times 2\pi k \end{cases}, \tag{16}$$

where the term $2\pi k$ appears in 2D cases due to the integration of the isotropic spectrum over the wavenumber sphere surface [1, 51]. By substituting Eqs. (9) and (13) into Eq. (16), one can yield the energy spectrum of equilibrium thermal fluctuations as

$$E_{eq}(k) = \begin{cases} \text{1D}: \frac{1}{2}\frac{k_B\langle T\rangle}{V_{cell}\langle\rho\rangle} \\ \text{2D}: \frac{k_B\langle T\rangle}{V_{cell}\langle\rho\rangle} \times 2\pi k \end{cases}. \tag{17}$$

Therefore, it can be concluded that for gases at thermodynamic equilibrium, the 1D energy spectrum is independent of the wavenumber k, while the 2D energy spectrum grows linearly with k. Extending this to the 3D cases will lead to the conclusion that $E_{eq}(k)$ grows quadratically with k [4, 9, 35, 51]. Similarly, the spectra of fluctuating thermodynamic variables can be written as

$$E_g(k) = \begin{cases} \text{1D}: \mathcal{F}\{\mathcal{R}_g\} \\ \text{2D}: \mathcal{F}\{\mathcal{R}_g\} \times 2\pi k \end{cases}, \tag{18}$$

where g stands for the number density, temperature, or pressure. Substituting Eqs. (10) - (13) into Eq. (18) would lead to the same conclusion that the equilibrium spectra of thermodynamic variables are independent of k for 1D cases, while they grow linearly with k for 2D cases.

It should be noted that the above derivations hold exactly for physical real gases. Since in DSMC simulations, each simulated molecule generally represents F real molecules, this will lead to larger thermal fluctuations due to the limited number of simulated molecules [33, 35, 49]. This problem can be subtly circumvented in 1D and 2D simulations as follows. The simulation ratio F is defined as

$$F = \frac{\langle n \rangle V_{cell}}{\langle N_p \rangle} = \frac{\langle n \rangle}{\langle N_p \rangle} \frac{L_x L_y L_z}{(N_c)^d}, \tag{19}$$

where $\langle N_p \rangle$ stands for the average number of simulated molecules in each DSMC cell, and d represents the dimension of the simulation. We assume that the values of $\langle n \rangle$, $\langle N_p \rangle$ and N_c are fixed in Eq. (19). Therefore, for the simulations of 1D turbulence, while L_y is fixed, we can control the values of L_x and L_z to set $F = 1$. Similarly, for the simulations of 2D turbulence, while L_x and L_y are fixed, we can vary the value of L_z to set $F = 1$. In this way, for both 1D and 2D simulations, each simulated molecule represents exactly one real molecule, and the DSMC method can reflect the thermal fluctuations of the real gas.

3 One-dimensional stationary turbulence

3.1 Simulation details

In this section, we employ the DSMC method to simulate the 1D stationary homogeneous compressible turbulence under large-scale forcing [52]. All the simulations are performed at $\langle T \rangle = 300\,\mathrm{K}$ and $\langle \rho \rangle = 1.6\,\mathrm{kg/m^3}$, where $\langle T \rangle$ and $\langle \rho \rangle$ are the mean values of temperature and mass density, respectively. Based on these parameters, the molecular mean collision time τ as well as the molecular mean free path λ_{mic} can be calculated, and thus the Knudsen number $Kn = \lambda_{mic}/L_y$ is determined, where L_y is the simulation domain length in the y direction (see Fig. 1). Following the discussions in Section 2.2, the domain lengths of the other two directions (L_x, L_z) are set equal, and they are controlled to set the DSMC simulation ratio $F = 1$. To ensure the simulation accuracy, the simulation time step Δt is equal to 0.1τ and the simulation cell length $L_{cell} = L_y/N_c$ is smaller than λ_{mic}.

During one simulation time step, a velocity increment $f_y \Delta t$ is added to the y component velocity of each molecule, where f_y is the acceleration caused by the external force. For this specific case, f_y is assumed to be Gaussian with zero-mean and white-in-time covariance as [52, 53]

$$f_y = \sum_{k_y=1}^{10} A(k_y) \left[a_{k_y} \sin\left(k_y \frac{y}{L_0} \right) + b_{k_y} \cos\left(k_y \frac{y}{L_0} \right) \right], \tag{20}$$

where $k_y = k/k_{\min}$ denotes the wavenumber index, $k_{\min} = 2\pi/L_y$ is the minimum wavenumber in simulations, and $L_0 = L_y/2\pi$ is the reference length. a_{k_y} and b_{k_y} are independent Gaussian random variables with zero mean and unit variance. The acceleration amplitude $A(k_y)$ is expressed as [52, 53]

$$A(k_y) = k_y \left[\exp(-{k_y}^2/{n_f}^2)/\tau_f \right]^{\frac{1}{2}}, \tag{21}$$

where n_f is the wavenumber index at which the amplitude has peak values, and τ_f denotes the force renewal time nondimensionalized by $V_{y,0}/L_0$, where $V_{y,0} = 600\,\mathrm{m/s}$ is the reference y-component velocity. In our simulations, we set $n_f = 5$, and vary τ_f to change the force magnitude. Note that Eq. (20) takes the dimensionless form, and it needs to be multiplied by ${V_{y,0}}^2/L_0$ to obtain the real accelerations exerted on the molecules.

As mentioned in Section 2.1, the periodic boundary condition is assumed for the simulation domain. The initial conditions are $(T/\langle T\rangle,\ \rho/\langle\rho\rangle,\ u_y/V_{y,0}) = (1,1,1)$ for the local macroscopic variables. Driven by the external force, the velocity field will form shock wave structures, which are the typical features of the 1D Burgers turbulence [52, 53]. To keep the turbulence at the stationary state, the thermostat needs to be implemented in our simulations to prevent the temperature increase due to the turbulence viscosity dissipation. Specifically, after molecular motions are completed in each time step, the global macroscopic velocity $\vec{V}$ and temperature T_g are obtained by sampling the molecular information. Then, the molecular velocity $\vec{c}$ for each molecule is scaled to get the new velocity $\vec{c}^*$ as [54]

$$\frac{c_i^* - V_{i,0}}{c_i - V_i} = \sqrt{\frac{\langle T\rangle}{T_g}}, \tag{22}$$

where $\vec{V}_0 = \left(V_{x,0}, V_{y,0}, V_{z,0}\right)$ is the reference global velocity.

After the turbulent velocity field reaches the stationary state, the turbulent statistical properties are obtained by spatial and temporal average. Specifically, TKE is defined as $K_{turb} = 0.5(u')^2$, where $u' = \left\langle (\delta u_y)^2 \right\rangle^{0.5}$ is the root mean square value of turbulent velocity fluctuations. The turbulent Mach number is defined as

$$M_t = \frac{u'}{\langle c\rangle}, \tag{23}$$

where $\langle c\rangle = \left\langle \sqrt{\gamma RT} \right\rangle$ is the mean speed of sound. The mean dissipation rate ε is calculated as

$$\varepsilon = \left\langle \frac{4}{3}\nu \left(\frac{\partial u_y}{\partial y}\right)^2 \right\rangle, \tag{24}$$

and then the Kolmogorov length scale η can be estimated (see Eq. (1)). The Taylor microscale λ and the corresponding Reynolds number Re_λ are defined as [52]

$$\lambda = \frac{u'}{\left\langle \left(\partial u_y/\partial y\right)^2 \right\rangle^{0.5}},\ Re_\lambda = \frac{u'\lambda}{\langle\nu\rangle}. \tag{25}$$

Define $L_T = {K_{turb}}^{3/2}/\varepsilon$ as the characteristic length scale of the large eddies, and thus the turbulent Reynolds number can be estimated as $Re_T = K_{turb}^{0.5} L_T/\langle\nu\rangle$ [1].

Note that Eqs. (24) and (25) are originally defined based on the deterministic NS equations. The stochastic noise inherent in DSMC simulations should be reduced to accurately calculate the velocity gradient [14]. Specifically, the above turbulent statistical properties are obtained based on the "coarse-grained" cells, rather than the original cells for DSMC simulations. The number of the coarse-grained cell N_g is much smaller than the original cell number N_c, so that the signal-to-noise ratio is greatly enhanced to an acceptable level [16]. Meanwhile, we ensure that the resolution parameter $k_{g,\max}\eta > 3.3$, where $k_{g,\max} = \pi N_g/L_y$ denotes the largest wavenumber corresponding to the half of N_g. Previous studies based on the DNS method have shown that the resolutions of $k_{g,\max}\eta > 2.0$ are sufficient for obtaining the convergent small-scale statistics in highly

Table 2 Simulated parameters and flow statistics for 1D stationary turbulence. All the simulations are performed at $\langle T \rangle = 300\,\mathrm{K}$ and $\langle \rho \rangle = 1.6\,\mathrm{kg/m^3}$

Case	$Kn\,(10^{-4})$	M_t	τ_f	L_y (mm)	N_c	$\langle N_p \rangle$	N_g	Re_T	Re_λ	$k_{g,\max}\eta$
A	0.71	0.53	0.08	0.8	16384	1500	2048	652.5	66.6	5.43
B	2.84	0.52	0.27	0.2	4096	2500	512	148.7	31.4	3.73
C	2.84	0.34	0.6	0.2	4096	2500	512	80.0	21.5	4.56
D	2.84	0.19	1.8	0.2	4096	2500	256	43.1	15.3	3.35

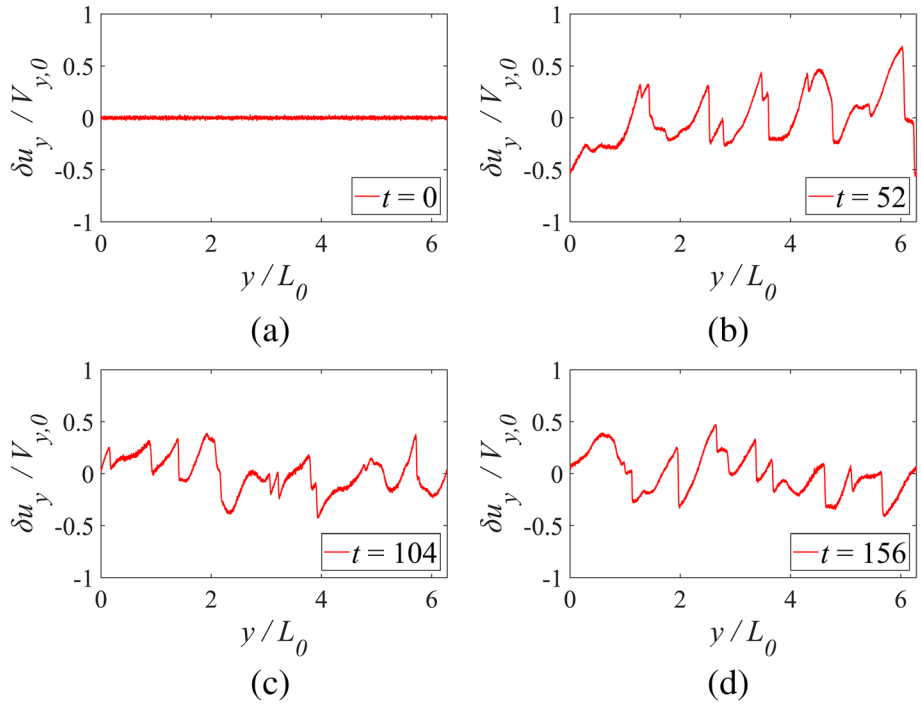

Fig. 2 Snapshots of velocity fluctuations for the Case B

compressible isotropic turbulence [40, 55]. Therefore, it is believed that the turbulent statistics obtained from the coarse-grained cells are comparable to those obtained from the DNS method. The simulated parameters and the corresponding flow statistics are shown in Table 2.

3.2 Numerical results

Figure 2 shows the spatial distributions of velocity fluctuations at four instants for the Case B, where the time t is nondimensionalized by the large eddy turnover time $\tau_T = L_T/u'$. At the beginning of the simulation, the velocity fluctuations are entirely caused by the thermal fluctuations, which are negligible compared to the reference velocity $V_{y,0}$ (see Fig. 2(a)). Then, driven by the large-scale force, the velocity field shows the typical shock wave structures, which are consistent with those obtained from the DNS method [52].

To further verify our simulations, we calculate the turbulent kinetic energy spectrum as

$$E(k) = \frac{1}{2}\frac{1}{N_c}\left|\mathcal{F}\{\delta u_y\}\right|^2. \tag{26}$$

Figure 3(a) shows the energy spectra for cases A and B, whose Knudsen numbers are different due to the change of the simulation domain length L_y. The abscissa in Fig. 3(a) is the wavenumber index k_y. It can be seen that the energy spectra for both cases show an inertial range with the scaling law close to k^{-2}, corresponding to the Burgers-like shock wave structures of the velocity field [52]. Besides, the spectrum of case A shows a longer inertial range than that of the case B, because the former owns a larger Re_λ (see Table 2).

More interestingly, it can be observed from Fig. 3(a) that, as k_y increases the spectra no longer vary with k_y, which is the feature of thermal fluctuations. As shown in Fig. 3(b), where the abscissa is the wavenumber k multiplied by the Kolmogorov length scale η, the DSMC calculated spectra at large wavenumbers agree well with the theoretical spectra predicted from Eq. (17). We can further define k_c as the crossover wavenumber [9, 35], beyond which the thermal fluctuations dominate the energy spectra. As can be seen from Fig. 3(b), for both cases A and B, k_c occurs at $k_c\eta \approx 6.5$, or $\eta/l_c \approx 1.03$ ($l_c = 2\pi/k_c$), which indicates that the thermal fluctuations have significant effects at spatial scales comparable to the Kolmogorov length scale. It is worth noting that similar conclusions were also reported by McMullen et al. [35] and Bell et al. [9] in their simulations of 3D turbulence, where they found k_c occurs at $\eta/l_c \approx 0.5$.

In Fig. 4, we compare the energy spectra for B, C and D cases, whose Knudsen numbers are the same, while the turbulent Mach numbers are different due to the change of the force magnitude. It can be seen from Table 2 that as M_t increases, the turbulent Reynolds number also increases. Since these three cases have the same equilibrium conditions, their energy spectra converge to the same spectrum of thermal

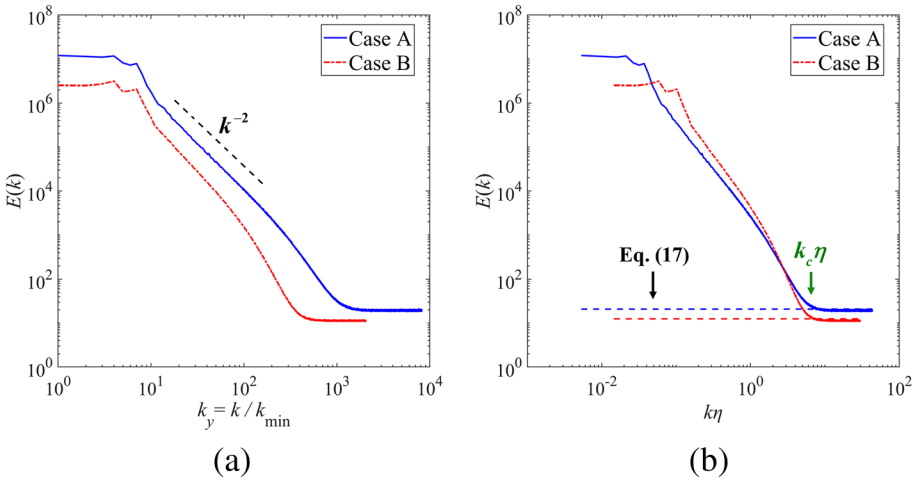

Fig. 3 The energy spectra of 1D compressible turbulence in the A and B cases. The abscissa of panel (a) is the wavenumber index, and the abscissa of panel (b) is the wavenumber multiplied by the Kolmogorov length scale. The spectra of thermal fluctuations calculated from Eq. (17) are also shown in panel (b) for comparison

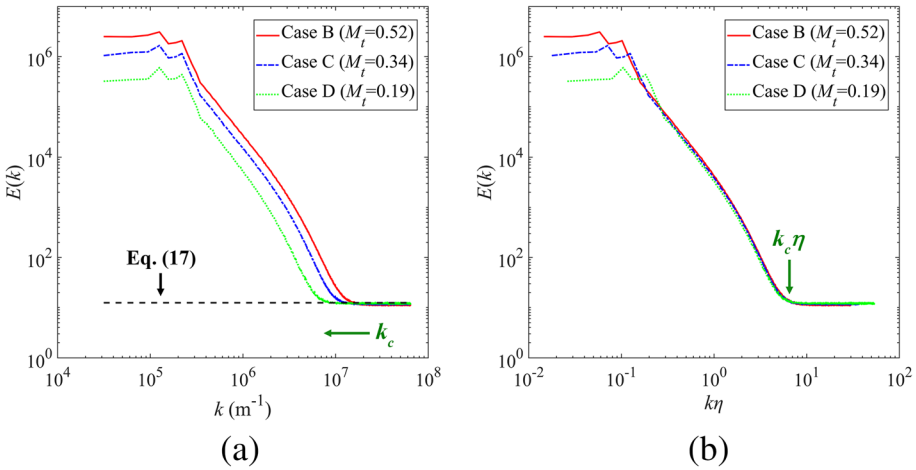

Fig. 4 The energy spectra of 1D compressible turbulence in the B, C and D cases. The abscissa of panel (a) is the wavenumber, and the abscissa of panel (b) is the wavenumber multiplied by the Kolmogorov length scale. The spectrum of thermal fluctuations calculated from Eq. (17) is also shown in panel (a) for comparison

fluctuations with the increase of wavenumber. Meanwhile, Fig. 4(a) shows that as M_t decreases, the crossover wavenumber k_c also decreases. This phenomenon can be qualitatively explained as follows: k_c represents the wavenumber at which the energy of turbulent velocity fluctuations balances with the energy of thermal velocity fluctuations [9, 14]. As can be seen in Fig. 4(a), the cases with lower M_t also own the lower TKE, and thus their energy spectra would reach the spectrum of thermal fluctuations at a lower wavenumber.

While the crossover wavenumbers are different for cases B to D, it is interesting to find in Fig. 4(b), that the values of $k_c\eta$ are almost the same. This is due to the fact that in our simulations, both l_c and η increase as the decrease of M_t. To summarize, the energy spectra of 1D turbulence are greatly affected by the thermal fluctuations at spatial scales comparable to the 3D cases [9, 35], but the spectral scaling law of thermal fluctuations (k^0) is different from that of 3D (k^2).

4 Two-dimensional decaying turbulence

4.1 Simulation details

In this section, we extend the DSMC simulations to the 2D decaying isotropic turbulence. Following the discussions in Section 2.2, we set $L_x = L_y = L$ for turbulence simulations (see Fig. 1), while we control the value of L_z to set the simulation ratio $F = 1$. The numbers of simulation cells N_c divided in the x and y directions are the same. The initial values of density, temperature, and pressure are taken to be uniform in the whole simulation domain, while the initial divergence-free velocity field follows the special form of the energy spectrum as [56–58]

$$E(k) = \frac{a_s}{2}\frac{(u_0')^2}{k_p}\left(\frac{k}{k_p}\right)^{2s+1}\exp\left[-(s+\frac{1}{2})\left(\frac{k}{k_p}\right)^2\right],\ a_s = \frac{(2s+1)^{s+1}}{2^s s!}, \tag{27}$$

where $u_0' = \left\langle \delta u_{x,0}{}^2 + \delta u_{y,0}{}^2 \right\rangle^{0.5}$ is the initial root mean square value of turbulent velocity fluctuations, s is a shape parameter of the spectrum, and k_p is the wavenumber at which the spectrum has peak values. In this work we take $s = 3$ and $k_p = 9k_{\min}$, where $k_{\min} = 2\pi/L$ is the minimum wavenumber. The macroscopic velocity $\vec{u}$ is randomly generated for each cell using the transfer procedures provided by Ishiko et al. [56].

Following the initial energy spectrum, the evolution of the velocity field is characterized by the vortex interactions, generating the so-called "direct enstrophy cascade" [57, 59, 60]. During the simulations, the turbulent statistical properties at different time instants are obtained by spatial average. The ensemble average can be further employed for independent runs following the same initial conditions. Specifically, TKE and M_t are calculated using the same equations as 1D turbulence. The enstrophy and its dissipation rate are defined as [60, 61]

$$\Omega = 0.5\left\langle |\vec{\omega}_u|^2 \right\rangle, \ \varepsilon_\Omega = 2\langle \nu \rangle P_\Omega, \tag{28}$$

respectively, where $\vec{\omega}_u = \nabla \times \vec{u}$ is the vorticity, and $P_\Omega = 0.5\left\langle |\nabla \times \vec{\omega}_u|^2 \right\rangle$ is the palinstrophy. The Taylor microscale and the corresponding Reynolds number are defined as [61]

$$\lambda = (\langle \nu \rangle \Omega / \varepsilon_\Omega)^{0.5}, \ Re_\lambda = \Omega^{1.5}/\varepsilon_\Omega \ , \tag{29}$$

respectively. The enstrophy dissipation length scale is defined as [59, 61]

$$\eta_\Omega = \left(\langle \nu \rangle^3 / \varepsilon_\Omega \right)^{1/6}, \tag{30}$$

in analogy with the Kolmogorov length scale. The global Reynolds number is defined as $Re = u' L_0 / \langle \nu \rangle$, where L_0=$L/2\pi$ is the reference length scale. Similar to 1D turbulence simulations, the turbulent statistics above are also obtained on the coarse-grained cells to reduce the stochastic noise.

In order to isolate the effect of compressibility, the Helmholtz decomposition [40–43] is applied to the macroscopic velocity field as

$$\vec{u} = \vec{u}^s + \vec{u}^c, \tag{31}$$

where the solenoidal component $\vec{u}^s$ and the compressible component $\vec{u}^c$ satisfy conditions $\nabla \cdot \vec{u}^s = 0$ and $\nabla \times \vec{u}^c = 0$, respectively. The turbulent kinetic energy for the solenoidal and compressible component can be further defined as $K^s_{turb} = 0.5\left\langle (\delta u^s_x)^2 + (\delta u^s_y)^2 \right\rangle$ and $K^c_{turb} = 0.5\left\langle (\delta u^c_x)^2 + (\delta u^c_y)^2 \right\rangle$, respectively.

Table 3 Simulated parameters and flow statistics for 2D decaying turbulence at $t = 3$. All the simulations are performed with the initial conditions of $T_0 = 300$ K, $P_0 = 1$ bar and $\rho_0 = 1.6$ kg/m^3

Case	Kn_0 (10^{-4})	M_{t0}	M_t	$\langle T \rangle$ (K)	L (mm)	N_c^2	$\langle N_p \rangle$	N_g^2	***Re***	Re_λ	$k_{g,\max}\eta_\Omega$
E	2.5	0.25	0.12	308	0.227	4096^2	25	64^2	94.8	4.5	2.37
F	2.5	0.5	0.29	326	0.227	4096^2	25	128^2	231.7	5.9	3.00
G	2.5	1	0.48	412	0.227	4096^2	25	128^2	351.4	7.4	2.45

Table 3 shows the simulated parameters and the corresponding turbulent statistics for $t = 3$, where t is the simulation time nondimensionalized by u_0'/L_0. Kn_0 and M_{t0} denote the initial Knudsen number and turbulent Mach number, respectively. Note that in comparison to the 1D and 3D turbulence, Re_λ shown in Table 3 is rather small corresponding to the direct enstrophy cascade in 2D turbulence [39]. To ensure the DSMC simulation accuracy, the simulation time step Δt is smaller than 0.2τ, and the simulation cell length $L_{cell} = L/N_c$ is smaller than λ_{mic}, where τ and λ_{mic} are the molecular mean collision time and the mean free path estimated based on the spatial mean values of temperature and density.

4.2 Basic features

Figure 5 shows the temporal evolution of the total kinetic energy K_{turb} and enstrophy Ω for the case G. Since the Reynolds number is small in our simulations, the decay rate of K_{turb} is larger than that in high-Reynolds-number turbulence [56, 58] due to the stronger effect of the viscous dissipation. Meanwhile, at $t \approx 10$, K_{turb} drops by 83%, while Ω drops by as much as 98%. The similar phenomenon is also found in the incompressible cases [56], as the decay rate of K_{turb} is bounded by the value of Ω [60, 61].

We define the compressibility factor χ as the ratio of the compressible kinetic energy K_{turb}^c to the total kinetic energy K_{turb}. As can be seen from Fig. 6, all the cases show $\chi = 0$ at the beginning of the simulation, corresponding to the divergence-free initial velocity field. Then, χ rapidly increases, which means that part of the solenoidal kinetic energy is converted into the compressible kinetic energy. As M_{t0} increases, the maximum value of χ increases from 0.02 to 0.13, which indicates that the compressible velocity component plays a more important role for a higher M_t.

Figures 7, 8 and 9 show the evolution of the vorticity field for cases E - G. It can be seen that the initial flow field consists of many small vortices, which are randomly distributed

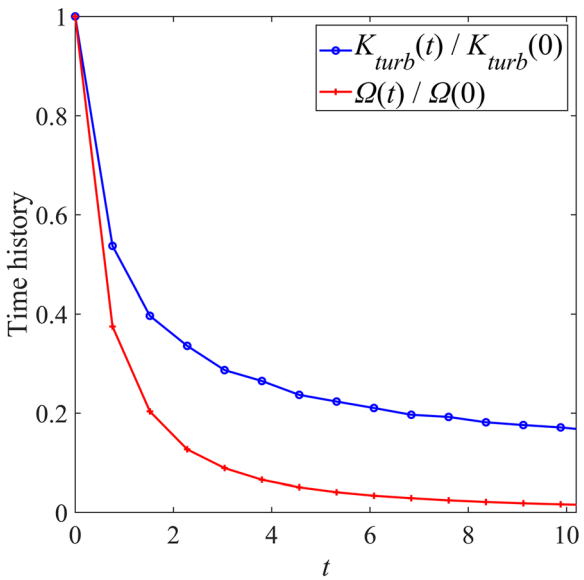

Fig. 5 Temporal evolution of the normalized turbulent kinetic energy and enstrophy for the case G

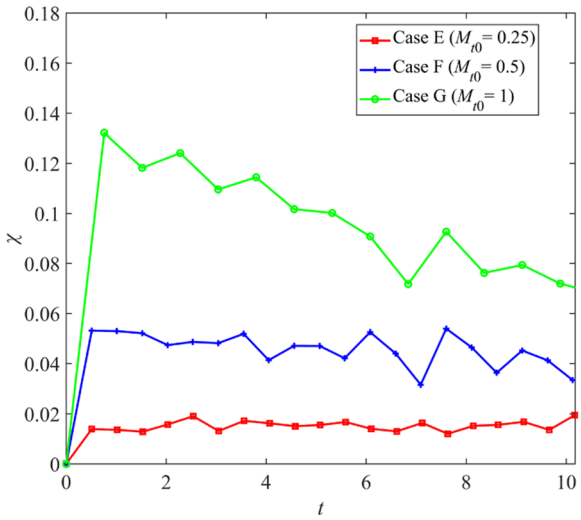

Fig. 6 Temporal evolution of the compressibility factor $\chi = K^c{}_{turb}/K_{turb}$ for cases E, F and G

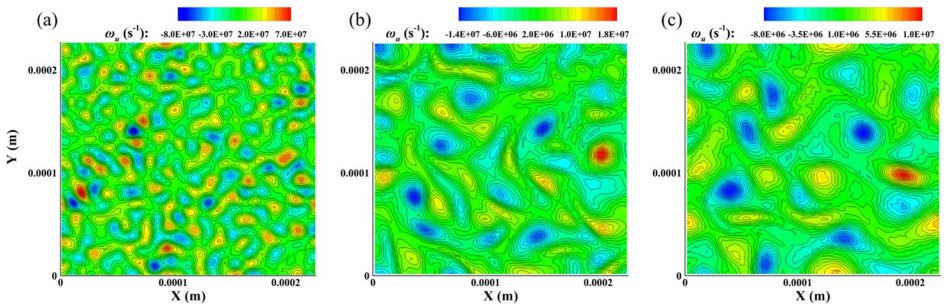

Fig. 7 Contours of the vorticity field for the case E at (a) $t = 0$, (b) $t = 3$, (c) $t = 6$

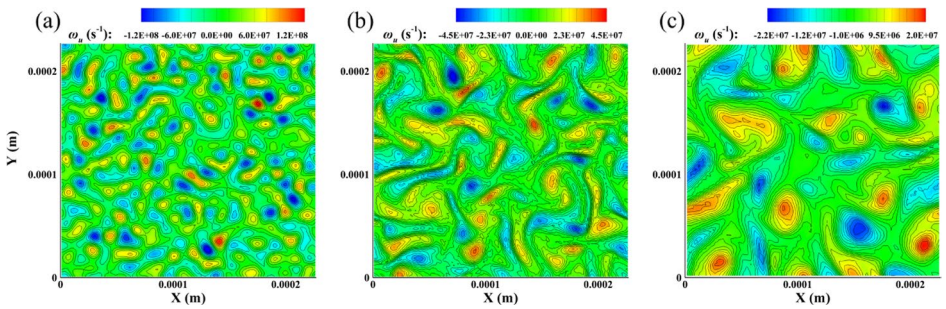

Fig. 8 Contours of the vorticity field for the case F at (a) $t = 0$, (b) $t = 3$, (c) $t = 6$

according to the initial energy spectrum. Then, the small vortices start to interact with each other to form the larger vortices, and the vorticity filaments can be observed [57, 62]. Besides, as M_t increases, there might be shock waves formed from the vortex interactions (see Fig. 9(b)), which in turn will significantly change the vortex structure. To further verify the presence of shock waves, the contours of the normalized values of density $\rho/\langle\rho\rangle$, temperature $T/\langle T\rangle$, and pressure $P/\langle P\rangle$ for the case G at $t = 3$ are shown in Fig. 10, where the severe discontinuities indicate the jumps of thermodynamic variables

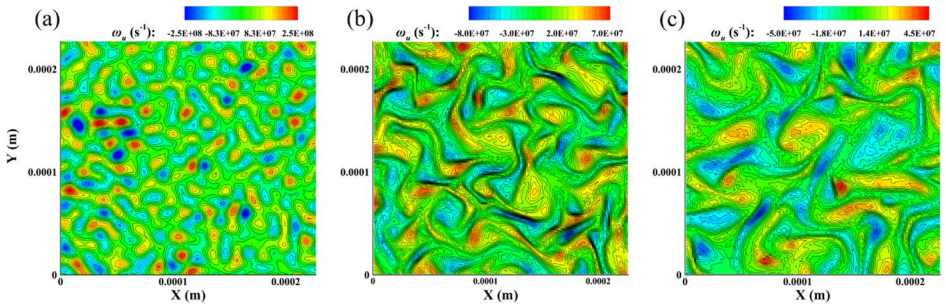

Fig. 9 Contours of the vorticity field for the case G at (a) $t = 0$, (b) $t = 3$, (c) $t = 6$

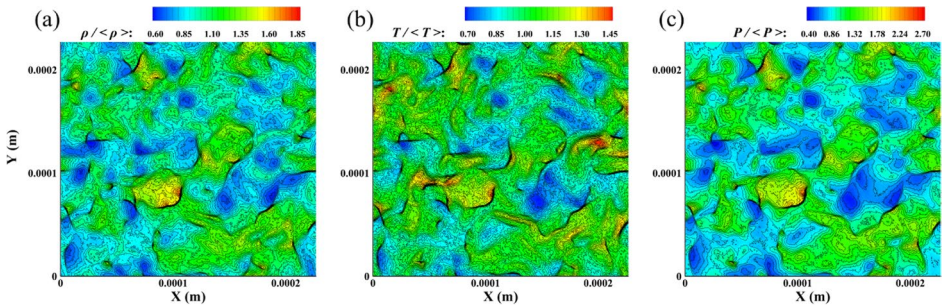

Fig. 10 Contours of the normalized density $\rho/\langle\rho\rangle$ (a), normalized temperature $T/\langle T\rangle$ (b), and normalized pressure $P/\langle P\rangle$ (c) for the case G at $t = 3$.

across the shock waves. Meanwhile, it can be observed that the fluctuations of $P/\langle P\rangle$ are stronger than those of $\rho/\langle\rho\rangle$ and $T/\langle T\rangle$. This phenomenon was also reported by Wang et al. [41] in their simulations of 3D compressible isotropic turbulence with shock waves.

The spectrum of the turbulent total kinetic energy is determined as

$$E(k) = \frac{\pi k}{{N_c}^2}\left(|\mathcal{F}\{\delta u_x\}|^2 + |\mathcal{F}\{\delta u_y\}|^2\right). \tag{32}$$

To reduce the statistical noise, a short-time average procedure is employed, i.e., the spectra are averaged over a time scale much smaller than the dissipation time scale $\tau_\Omega = \varepsilon_\Omega^{-1/3}$, but much larger than the molecular mean collision time. In Fig. 11, we compare the spectra for cases E, F, and G at $t = 3$. Note that the case with a higher M_t also corresponds to a higher *Re* (see Table 3). It can be seen from Fig. 11(a) that, as the increase of *Re*, $E(k)$ shows a more distinct inertial range, and its scaling law approaches the $k^{-3}[\ln(k)]^{-1/3}$ limit, in agreement with the Kraichnan-Batchelor-Leith (KBL) theory [57, 59, 63].

Figure 11(a) also shows that, as the wavenumber increases, the energy spectra grow linearly with k, which corresponds to the thermal fluctuations. As can be observed from Fig. 11(b), all the DSMC calculated spectra agree well with the theoretical spectra given by Eq. (17) at larger wavenumbers. The simulation case with a higher M_t has larger spectral values of thermal fluctuations due to the higher temperature rise (see Table 3). Comparing Fig. 11(a), (b), one can see that the crossover wavenumber k_c decreases significantly as the decrease of M_t, but its product with the enstrophy dissipation length scale η_Ω does not change significantly. The $k_c\eta_\Omega$ lies between 2.2 and 4, corresponding to

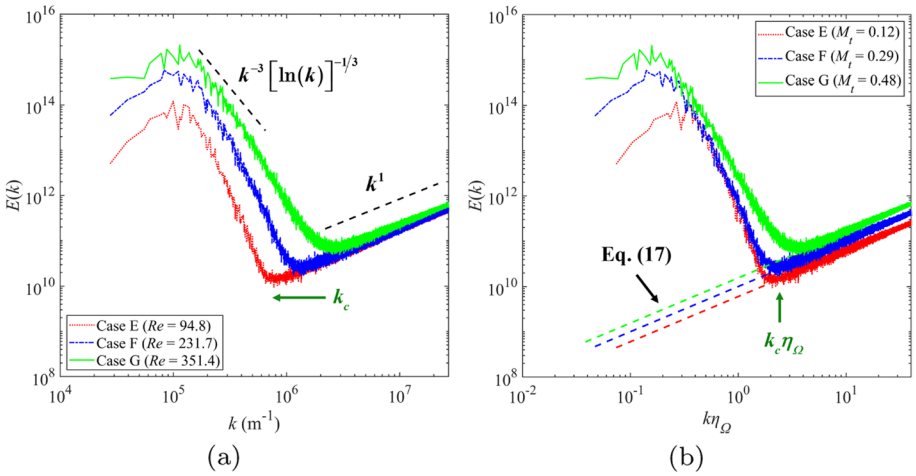

Fig. 11 The energy spectra of 2D decaying compressible turbulence in the E, F and G cases at $t = 3$. The abscissa of panel (a) is the wavenumber, and the abscissa of panel (b) is the wavenumber multiplied by the enstrophy dissipation length scale. The spectra of thermal fluctuations calculated from Eq. (17) are also shown in panel (b) for comparison

η_Ω / l_c in the range of 0.35 to 0.64, indicating that the thermal fluctuations dominate the spectra at spatial scales slightly larger than the dissipation length scale.

4.3 Effect of compressibility on spectra

In the previous sections, our simulation results for both 1D and 2D turbulence show that the thermal fluctuations dominate the turbulent kinetic energy spectra at spatial scales comparable to the viscous dissipation length scale, which is in good agreement with the previous conclusion on 3D turbulence [9, 35]. In this subsection, we extend our simulations of 2D turbulence to study the effect of compressibility on the interactions between thermal fluctuations and turbulence.

To start with, we decompose the total energy spectrum $E(k)$ into the spectra of solenoidal and compressible velocity component, denoted by $E^s(k)$ and $E^c(k)$ respectively, in order to separate the effects of thermal fluctuations. In Fig. 12, we present the instantaneous results of $E(k)$, $E^s(k)$ and $E^c(k)$ for cases E - G at $t = 3$. As can be seen from Fig. 12, $E^s(k)$ almost overlaps with $E(k)$ in the range of $k\eta_\Omega < 1.2$, corresponding to the relatively small values of the compressibility factor χ. As M_t increases, the intensity of $E^c(k)$ increases significantly, and the spectra show an inertial range with the scaling law close to k^{-2}. Note that the reported inertial scaling law of $E^c(k)$ for the 2D compressible turbulence remains controversial in the literature. While some researches reported the inertial spectra steeper than k^{-2} [36, 39], a recent numerical study by Kritsuk [64] shows that the inertial scaling law is close to k^{-2}, which corresponds to the acoustic waves in turbulence. Since in our simulations, the flow field is characterized by shock wave structures at a higher M_t (see Fig. 10), it is reasonable that $E^c(k)$ forms a scaling law close to k^{-2} [41].

As can be seen from Fig. 12, both $E^s(k)$ and $E^c(k)$ grow linearly with k at large wavenumbers, which is the typical feature of thermal fluctuations. In order to study the effect of thermal fluctuations under different M_t, we define ${k_c}^s$ and ${k_c}^c$ as the crossover

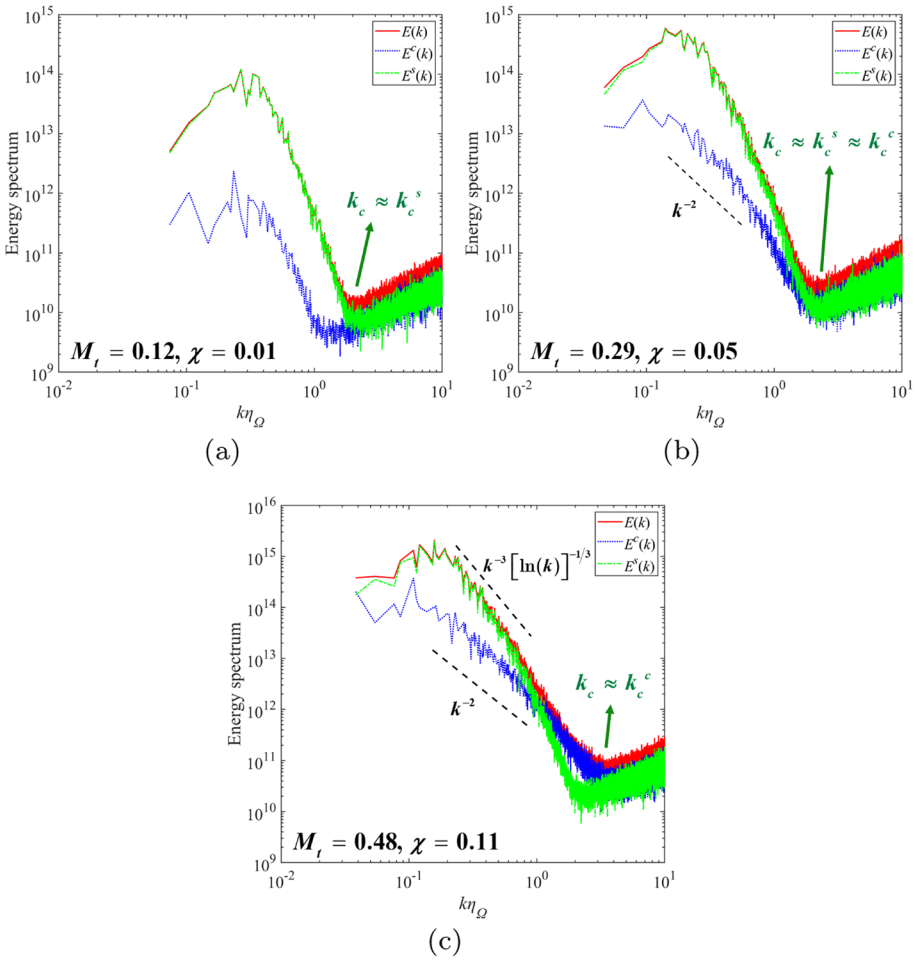

Fig. 12 Energy spectra for the velocity field and its two components at $t = 3$, for the case (a) E, (b) F and (c) G

wavenumbers correspond to $E^s(k)$ and $E^c(k)$, respectively. As M_t increases, ${k_c}^s\eta_\Omega$ remains unchanged around 2.2, indicating that the effect of thermal fluctuations on $E^s(k)$ is insensitive to the change of compressibility. However, this conclusion does not hold for $E^c(k)$, as ${k_c}^c\eta_\Omega$ changes significantly from 1.3 to 4 as the increase of M_t. Specifically, at $M_t = 0.12$, the compressibility factor χ is so small that $E^c(k)$ decays rapidly, leading to a lower ${k_c}^c\eta_\Omega$. As M_t increases, $E^c(k)$ gets closer to $E^s(k)$ (see Fig. 12(b) for $M_t = 0.29$) , and then $E^c(k)$ will dominate the energy content at high wavenumbers (see Fig. 12(c) for $M_t = 0.48$), as expected for the highly compressible turbulence [55, 64]. Consequently, ${k_c}^c$ gradually exceeds ${k_c}^s$ as M_t increases. The crossover wavenumber k_c for the total energy spectrum $E(k)$ is always determined as the larger value between ${k_c}^s$ and ${k_c}^c$, as shown in Fig. 12.

Since the compressible turbulence owns distinguishing features of the fluctuations in thermodynamic variables [38–43], it is of great interest to study the effect of thermal fluctuations on the spectra of thermodynamic variables under different M_t. We calculate the thermodynamic spectra as

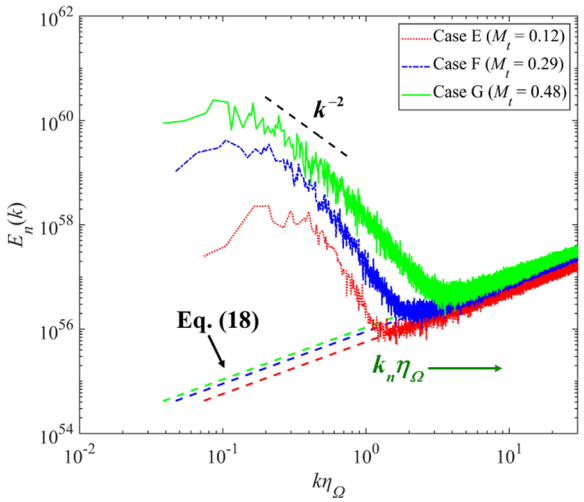

Fig. 13 Spectra of number density fluctuations for the cases E, F and G at $t = 3$. The spectra of thermal fluctuations calculated from Eq. (18) are also shown for comparison

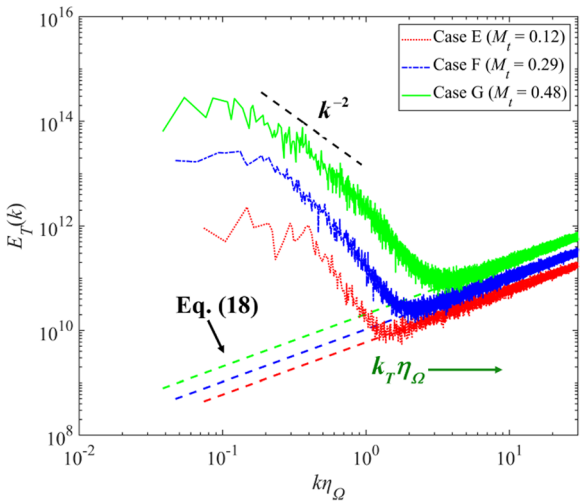

Fig. 14 Spectra of temperature fluctuations for the cases E, F and G at $t = 3$. The spectra of thermal fluctuations calculated from Eq. (18) are also shown for comparison

$$E_g(k) = \frac{2\pi k}{{N_c}^2}\left|\mathcal{F}\{\delta g\}\right|^2, \tag{33}$$

where g stands for the number density n, temperature T, or pressure P. Figures 13, 14 and 15 show the results of $E_n(k)$, $E_T(k)$ and $E_P(k)$ for cases E - G at $t = 3$. As M_t increases, the spectra for the three thermodynamic variables show the same inertial range scaling law close to k^{-2}. As the increase of wavenumber, the thermodynamic spectra grow linearly with k, corresponding to the thermal fluctuations. The DSMC results are in good agreement with the spectra of thermal fluctuations calculated from Eq. (18) at large wavenumbers. We define the crossover wavenumbers for the density, temperature, and

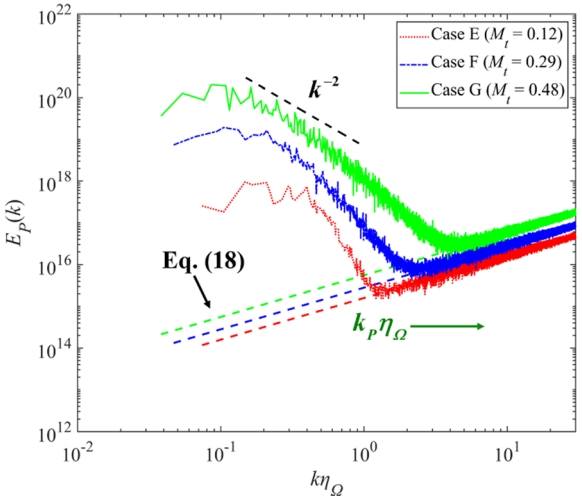

Fig. 15 Spectra of pressure fluctuations for the cases E, F and G at $t = 3$. The spectra of thermal fluctuations calculated from Eq. (18) are also shown for comparison

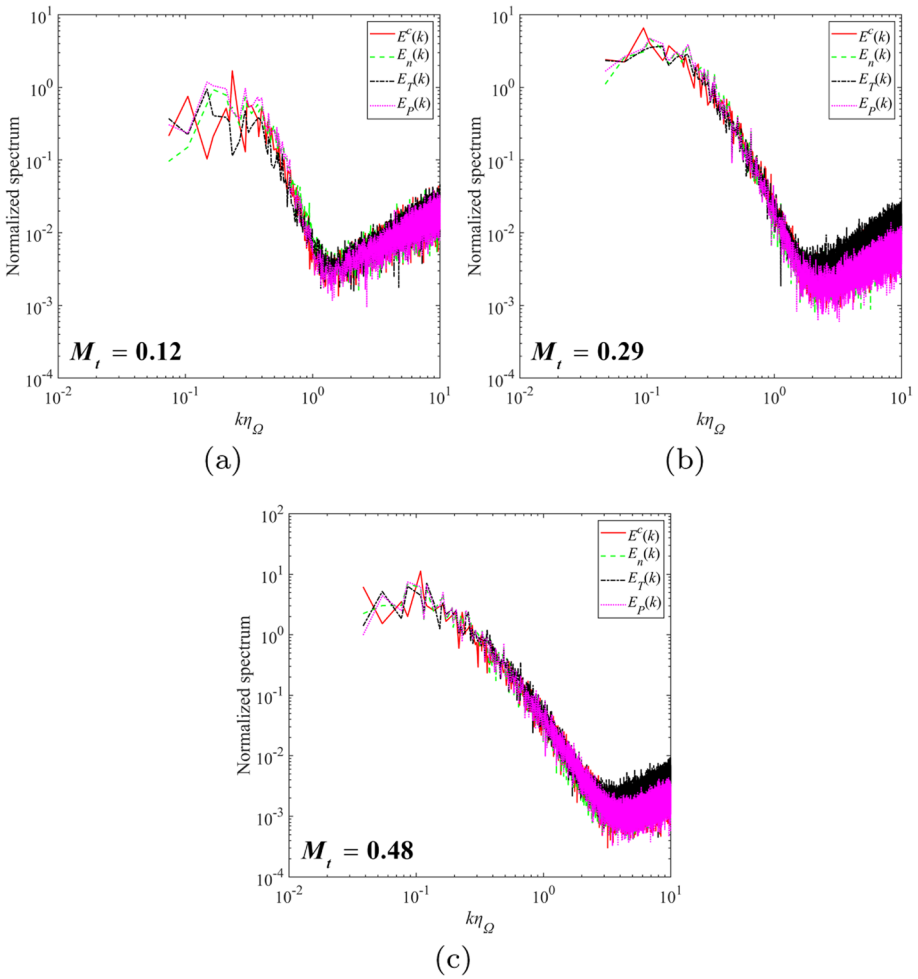

Fig. 16 Normalized spectra of the compressible velocity component, number density, temperature, and pressure at $t = 3$, for the case (a) E, (b) F, and (c) G

pressure as k_n, k_T, and k_P. It is interesting to find that all the values of $k_n\eta_\Omega$, $k_T\eta_\Omega$, and $k_P\eta_\Omega$ increase from 1.3 to 4 as M_t increases, which is consistent with the aforementioned trend for ${k_c}^c\eta_\Omega$. To further verify the coupling relationship between the spectra of thermodynamic variables and the spectrum of compressible velocity component, we compare the instantaneous spectra in Fig. 16 under different M_t, following the normalized rules that the integral of the spectrum over the entire wavenumber range is equal to 1. It can be seen that all the spectra of thermodynamic variables are consistent with $E^c(k)$, indicating that the spatial correlations of thermodynamic fluctuations are dominated by the compressible mode of the velocity field. In this way, the effects of thermal fluctuations on the turbulence thermodynamic spectra under different M_t are the same as those on $E^c(k)$.

5 Concluding remarks

In this work, we employed the DSMC method to simulate 1D stationary homogeneous turbulence and 2D decaying isotropic turbulence at the molecular level, in order to study the effect of thermal fluctuations on turbulence under different turbulent Mach numbers M_t. Our results show that the DSMC method can obtain the expected turbulent flow structures, and the spectral scaling laws of the inertial range are consistent with those obtained based on the deterministic NS equations. More interesting, the DSMC results predict that the turbulent energy spectra $E(k)$ are greatly affected by thermal fluctuations in the dissipation range, which obviously cannot be revealed by the deterministic NS equations.

It is found that the crossover length scale l_c at which the thermal fluctuations dominate $E(k)$ occurs in the same order of magnitude as the viscous dissipation length scale (η for 1D cases, and η_Ω for 2D cases), which shows good agreement with the previous conclusion on 3D turbulence [9, 35]. Meanwhile, the wavenumber scaling laws of the energy spectra caused by thermal fluctuations depend on the spatial dimensions d as $k^{(d-1)}$.

For 2D turbulence, we further decomposed $E(k)$ into the spectra of solenoidal and compressible velocity components, and the corresponding crossover wavenumbers (i.e., ${k_c}^s$ and ${k_c}^c$) were determined under different M_t. It is found that the values of ${k_c}^s\eta_\Omega$ are almost unchanged, while the values of ${k_c}^c\eta_\Omega$ increase significantly with M_t, indicating that the effect of thermal fluctuations on the spectrum of compressible velocity component is greatly affected by the change of compressibility.

We also calculated the spectra of density, temperature and pressure for 2D turbulence. The results show that all the thermodynamic spectra grow linearly with k at large wavenumbers, revealing the similar effect of thermal fluctuations as found for the energy spectra. More importantly, it is found that the thermodynamic spectra are dominated by the compressible mode of velocity field, leading to the fact that the crossover wavenumbers for the thermodynamic spectra are the same as ${k_c}^c$.

Together with the previous study [35], our work demonstrates that the DSMC method serves as a powerful tool to investigate the interactions between thermal fluctuations and turbulence, which cannot be described by the deterministic NS equations. While the present studies are limited to 1D and 2D cases, it will be of great interest to explore whether the conclusions we drawn can be extended to 3D cases in the future,

particularly for the compressibility effect. Previous studies of 3D turbulence have shown that the computational cost of the DSMC method would become notoriously large [31], so the multiscale stochastic particle methods, such as the particle Fokker-Planck method [54, 65] or the unified stochastic particle (USP) method [66, 67], are expected to investigate the effect of thermal fluctuations on compressible turbulence with higher computational efficiency.

Acknowledgements
The authors thank Prof. Guice Yao, Prof. Jian Yu, Peng Tian and Ziqi Cui for helpful discussions about this work.

Authors' contributions
The contribution of the authors to the work is equivalent. All authors read and approved the final manuscript.

Funding
This work was supported by the National Natural Science Foundation of China (Grant No. 92052104). The results were obtained on the Zhejiang Super Cloud Computing Center M6 Partition.

Availability of data and materials
All data generated or analyzed during this study are included in this published article.

Declarations

Competing interests
The authors declare that they have no competing interests.

Received: 1 November 2022 Accepted: 29 November 2022
Published online: 01 February 2023

References

1. Pope SB (2000) Turbulent flows. Cambridge University Press, Cambridge
2. Tennekes H, Lumley JL (1972) A first course in turbulence. MIT press, Cambridge, Massachusetts
3. Moser RD (2006) On the validity of the continuum approximation in high Reynolds number turbulence. Phys Fluids 18(7):078105
4. Betchov R (1957) On the fine structure of turbulent flows. J Fluid Mech 3(2):205–216
5. Betchov R (1964) Measure of the intricacy of turbulence. Phys Fluids 7(8):1160–1162
6. Landau LD, Lifshitz EM (1959) Fluid mechanics: course of theoretical physics, vol. 6. Pergamon Press, Oxford
7. Garcia AL, Mansour MM, Lie GC et al (1987) Numerical integration of the fluctuating hydrodynamic equations. J Stat Phys 47:209–228
8. de Zárate JMO, Sengers JV (2006) Hydrodynamic fluctuations in fluids and fluid mixtures. Elsevier, Amsterdam
9. Bell JB, Nonaka A, Garcia AL et al (2022) Thermal fluctuations in the dissipation range of homogeneous isotropic turbulence. J Fluid Mech 939:A12
10. Khurshid S, Donzis DA, Sreenivasan KR (2018) Energy spectrum in the dissipation range. Phys Rev Fluids 3(8):082601
11. Buaria D, Sreenivasan KR (2020) Dissipation range of the energy spectrum in high Reynolds number turbulence. Phys Rev Fluids 5(9):092601
12. Kraichnan RH (1967) Intermittency in the very small scales of turbulence. Phys Fluids 10(9):2080–2082
13. Chen S, Doolen G, Herring JR et al (1993) Far-dissipation range of turbulence. Phys Rev Lett 70(20):3051–3054
14. Bandak D, Goldenfeld N, Mailybaev AA et al (2022) Dissipation-range fluid turbulence and thermal noise. Phys Rev E 105(6):065113
15. Rapaport DC (2004) The art of molecular dynamics simulation, 2nd edn. Cambridge University Press, Cambridge
16. Smith ER (2015) A molecular dynamics simulation of the turbulent Couette minimal flow unit. Phys Fluids 27(11):115105
17. Bird GA (1994) Molecular gas dynamics and the direct simulation of gas flows. Clarendon Press, Oxford
18. Boyd ID, Schwartzentruber TE (2017) Nonequilibrium gas dynamics and molecular simulation. Cambridge University Press, Cambridge
19. Koura K, Matsumoto H (1991) Variable soft sphere molecular model for inverse-power-law or Lennard-Jones potential. Phys Fluids A Fluid Dyn 3(10):2459–2465
20. Wagner W (1992) A convergence proof for Bird's direct simulation Monte Carlo method for the Boltzmann equation. J Stat Phys 66(3):1011–1044
21. Garcia AL (1986) Nonequilibrium fluctuations studied by a rarefied-gas simulation. Phys Rev A 34(2):1454–1457
22. Mansour MM, Garcia AL, Lie GC et al (1987) Fluctuating hydrodynamics in a dilute gas. Phys Rev Lett 58(9):874–877
23. Bruno D, Capitelli M, Longo S et al (2006) Monte Carlo simulation of light scattering spectra in atomic gases. Chem Phys Lett 422:571–574
24. Zhang J, Fan J (2009) Monte Carlo simulation of thermal fluctuations below the onset of Rayleigh-Bénard convection. Phys Rev E 79(5):056302
25. Bruno D (2019) Direct simulation Monte Carlo simulation of thermal fluctuations in gases. Phys Fluids 31(4):047105

26. Ma Q, Yang C, Bruno D et al (2021) Molecular simulation of Rayleigh-Brillouin scattering in binary gas mixtures and extraction of the rotational relaxation numbers. Phys Rev E 104(3):035109
27. Manela A, Zhang J (2012) The effect of compressibility on the stability of wall-bounded Kolmogorov flow. J Fluid Mech 694:29–49
28. Gallis MA, Koehler TP, Torczynski JR et al (2015) Direct simulation Monte Carlo investigation of the Richtmyer-Meshkov instability. Phys Fluids 27(8):084105
29. Gallis MA, Koehler TP, Torczynski JR et al (2016) Direct simulation Monte Carlo investigation of the Rayleigh-Taylor instability. Phys Rev Fluids 1(4):043403
30. Plimpton SJ, Moore SG, Borner A et al (2019) Direct simulation Monte Carlo on petaflop supercomputers and beyond. Phys Fluids 31(8):086101
31. Gallis MA, Bitter NP, Koehler TP et al (2017) Molecular-level simulations of turbulence and its decay. Phys Rev Lett 118(6):064501
32. Gallis MA, Torczynski JR, Bitter NP et al (2018) Gas-kinetic simulation of sustained turbulence in minimal Couette flow. Phys Rev Fluids 3(7):071402
33. Gallis MA, Torczynski JR, Krygier MC et al (2021) Turbulence at the edge of continuum. Phys Rev Fluids 6(1):013401
34. McMullen R, Krygier M, Torczynski J et al (2022) Gas-kinetic simulations of compressible turbulence over a mean-free-path-scale porous wall. Paper presented at the AIAA SCITECH 2022 Forum, San Diego & Virtual, 3-7 January 2022
35. McMullen RM, Krygier MC, Torczynski JR et al (2022) Navier-Stokes equations do not describe the smallest scales of turbulence in gases. Phys Rev Lett 128(11):114501
36. Passot T, Pouquet A (1987) Numerical simulation of compressible homogeneous flows in the turbulent regime. J Fluid Mech 181:441–466
37. Andreopoulos Y, Agui JH, Briassulis G (2000) Shock wave—turbulence interactions. Annu Rev Fluid Mech 32(1):309–345
38. Donzis DA, Jagannathan S (2013) Fluctuations of thermodynamic variables in stationary compressible turbulence. J Fluid Mech 733:221–244
39. Terakado D, Hattori Y (2014) Density distribution in two-dimensional weakly compressible turbulence. Phys Fluids 26(8):085105
40. Wang J, Gotoh T, Watanabe T (2017) Spectra and statistics in compressible isotropic turbulence. Phys Rev Fluids 2(1):013403
41. Wang J, Wan M, Chen S et al (2018) Effect of shock waves on the statistics and scaling in compressible isotropic turbulence. Phys Rev E 97(4):043108
42. Chen S, Wang J, Li H et al (2018) Spectra and Mach number scaling in compressible homogeneous shear turbulence. Phys Fluids 30(6):065109
43. Wang J, Wan M, Chen S et al (2019) Cascades of temperature and entropy fluctuations in compressible turbulence. J Fluid Mech 867:195–215
44. Chen S, Stemmer C (2022) Modeling of thermochemical nonequilibrium flows using open-source direct simulation Monte Carlo kernel SPARTA. J Spacecr Rockets 59(5):1634–1646
45. Alexander FJ, Garcia AL, Alder BJ (1998) Cell size dependence of transport coefficients in stochastic particle algorithms. Phys Fluids 10(6):1540–1542
46. Hadjiconstantinou NG (2000) Analysis of discretization in the direct simulation Monte Carlo. Phys Fluids 12(10):2634–2638
47. Landau LD, Lifshitz EM (1980) Statistical physics, part 1. Pergamon Press, Oxford
48. Lifshitz EM, Pitaevskii LP (1980) Statistical physics, part 2. Pergamon Press, Oxford
49. Hadjiconstantinou NG, Garcia AL, Bazant MZ et al (2003) Statistical error in particle simulations of hydrodynamic phenomena. J Comput Phys 187(1):274–297
50. Press WH, Teukolsky SA, Vetterling WT et al (2007) Numerical recipes. The art of scientific computing. 3rd edn. Cambridge University Press, Cambridge
51. Verma MK (2020) Boltzmann equation and hydrodynamic equations: their equilibrium and non-equilibrium behaviour. Philos Trans Royal Soc A 378(2175):20190470
52. Ni Q, Shi Y, Chen S (2013) Statistics of one-dimensional compressible turbulence with random large-scale force. Phys Fluids 25(7):075106
53. Boldyrev S, Linde T, Polyakov A (2004) Velocity and velocity-difference distributions in Burgers turbulence. Phys Rev Lett 93(18):184503
54. Zhang J, Tian P, Yao SQ et al (2019) Multiscale investigation of Kolmogorov flow: From microscopic molecular motions to macroscopic coherent structures. Phys Fluids 31(8):082008
55. Wang J, Shi Y, Wang LP et al (2012) Effect of compressibility on the small-scale structures in isotropic turbulence. J Fluid Mech 713:588–631
56. Ishiko K, Ohnishi N, Ueno K et al (2009) Implicit large eddy simulation of two-dimensional homogeneous turbulence using weighted compact nonlinear scheme. J Fluids Eng 131(6):061401
57. San O, Staples AE (2012) High-order methods for decaying two-dimensional homogeneous isotropic turbulence. Comput Fluids 63:105–127
58. Yu J, Yan C, Jiang Z (2014) On the use of the discontinuous Galerkin method for numerical simulation of two-dimensional compressible turbulence with shocks. Sci China Phys Mech Astron 57(9):1758–1770
59. Kraichnan RH (1967) Inertial ranges in two-dimensional turbulence. Phys Fluids 10(7):1417–1423
60. Boffetta G, Ecke RE (2012) Two-dimensional turbulence. Ann Rev Fluid Mech 44(1):427–451
61. Herring JR, Orszag SA, Kraichnan RH et al (1974) Decay of two-dimensional homogeneous turbulence. J Fluid Mech 66(3):417–444
62. Kevlahan NKR, Farge M (1997) Vorticity filaments in two-dimensional turbulence: creation, stability and effect. J Fluid Mech 346:49–76
63. Kraichnan RH (1971) Inertial-range transfer in two- and three-dimensional turbulence. J Fluid Mech 47(3):525–535

64. Kritsuk AG (2019) Energy transfer and spectra in simulations of two-dimensional compressible turbulence. In: Gorokhovski M, Godeferd FS (eds) Turbulent cascades II. ERCOFTAC Series, vol 26. Springer, Cham
65. Zhang J, John B, Pfeiffer M et al (2019) Particle-based hybrid and multiscale methods for nonequilibrium gas flows. Adv Aerodyn 1(1):12
66. Fei F, Zhang J, Li J et al (2020) A unified stochastic particle Bhatnagar-Gross-Krook method for multiscale gas flows. J Comput Phys 400:108972
67. Fei F, Jenny P (2021) A hybrid particle approach based on the unified stochastic particle Bhatnagar-Gross-Krook and DSMC methods. J Comput Phys 424:109858

Publisher's Note